NASA/TM-2003-212021

Aeroservoelastic Model Validation and Test Data Analysis of the F/A-18 Active Aeroelastic Wing

Martin J. Brenner and Richard J. Prazenica
NASA Dryden Flight Research Center
Edwards, California

April 2003

The NASA STI Program Office…in Profile

Since its founding, NASA has been dedicated to the advancement of aeronautics and space science. The NASA Scientific and Technical Information (STI) Program Office plays a key part in helping NASA maintain this important role.

The NASA STI Program Office is operated by Langley Research Center, the lead center for NASA's scientific and technical information. The NASA STI Program Office provides access to the NASA STI Database, the largest collection of aeronautical and space science STI in the world. The Program Office is also NASA's institutional mechanism for disseminating the results of its research and development activities. These results are published by NASA in the NASA STI Report Series, which includes the following report types:

- TECHNICAL PUBLICATION. Reports of completed research or a major significant phase of research that present the results of NASA programs and include extensive data or theoretical analysis. Includes compilations of significant scientific and technical data and information deemed to be of continuing reference value. NASA's counterpart of peer-reviewed formal professional papers but has less stringent limitations on manuscript length and extent of graphic presentations.

- TECHNICAL MEMORANDUM. Scientific and technical findings that are preliminary or of specialized interest, e.g., quick release reports, working papers, and bibliographies that contain minimal annotation. Does not contain extensive analysis.

- CONTRACTOR REPORT. Scientific and technical findings by NASA-sponsored contractors and grantees.

- CONFERENCE PUBLICATION. Collected papers from scientific and technical conferences, symposia, seminars, or other meetings sponsored or cosponsored by NASA.

- SPECIAL PUBLICATION. Scientific, technical, or historical information from NASA programs, projects, and mission, often concerned with subjects having substantial public interest.

- TECHNICAL TRANSLATION. English-language translations of foreign scientific and technical material pertinent to NASA's mission.

Specialized services that complement the STI Program Office's diverse offerings include creating custom thesauri, building customized databases, organizing and publishing research results…even providing videos.

For more information about the NASA STI Program Office, see the following:

- Access the NASA STI Program Home Page at ***http://www.sti.nasa.gov***

- E-mail your question via the Internet to help@sti.nasa.gov

- Fax your question to the NASA Access Help Desk at (301) 621-0134

- Telephone the NASA Access Help Desk at (301) 621-0390

- Write to:
  NASA Access Help Desk
  NASA Center for AeroSpace Information
  7121 Standard Drive
  Hanover, MD 21076-1320

NASA/TM-2003-212021

Aeroservoelastic Model Validation and Test Data Analysis of the F/A-18 Active Aeroelastic Wing

Martin J. Brenner and Richard J. Prazenica
NASA Dryden Flight Research Center
Edwards, California

National Aeronautics and
Space Administration

Dryden Flight Research Center
Edwards, California 93523-0273

April 2003

NOTICE

Use of trade names or names of manufacturers in this document does not constitute an official endorsement of such products or manufacturers, either expressed or implied, by the National Aeronautics and Space Administration.

Available from the following:

NASA Center for AeroSpace Information (CASI)
7121 Standard Drive
Hanover, MD 21076-1320
(301) 621-0390

National Technical Information Service (NTIS)
5285 Port Royal Road
Springfield, VA 22161-2171
(703) 487-4650

ABSTRACT

Model validation and flight test data analysis require careful consideration of the effects of uncertainty, noise, and nonlinearity. Uncertainty prevails in the data analysis techniques and results in a composite model uncertainty from unmodeled dynamics, assumptions and mechanics of the estimation procedures, noise, and nonlinearity. A fundamental requirement for reliable and robust model development is an attempt to account for each of these sources of error, in particular, for model validation, robust stability prediction, and flight control system development. This paper is concerned with data processing procedures for uncertainty reduction in model validation for stability estimation and nonlinear identification.

F/A-18 Active Aeroelastic Wing (AAW) aircraft data is used to demonstrate signal representation effects on uncertain model development, stability estimation, and nonlinear identification. Data is decomposed using adaptive orthonormal best-basis and wavelet-basis signal decompositions for signal denoising into linear and nonlinear identification algorithms. Nonlinear identification from a wavelet-based Volterra kernel procedure is used to extract nonlinear dynamics from aeroelastic responses, and to assist model development and uncertainty reduction for model validation and stability prediction by removing a class of nonlinearity from the uncertainty.

INTRODUCTION

Aeroelastic and aeroservoelastic (ASE) flight data analysis and model validation must necessarily cope with uncertainty, noise, and nonlinearity. Model uncertainty between a high-fidelity computational model, reduced-order (ref. [1]) model, or a linear model, and a descriptive representation of the actual aircraft dynamics is inevitable. ASE systems comprise interactions of generally multi-input multi-output sampled-data control feedback with actuation dynamics coupled with ASE. Highly augmented closed-loop flight test data require extra care in distinguishing system component dynamics. Important considerations of uncertainty classification relative to the signal processing and identification procedures, versus an actual model mis-match, must be assessed and minimized for accurate model updates.

Identification of ASE dynamics presents one of the greatest challenges for flight data analysis. Unsteady aerodynamics, turbulence, shock effects, and spatially local behaviors are often difficult to quantify, especially with inadequate instrumentation. Exogenous inputs and asymmetric characteristics create problems for observability and identifiability. Model verification over an extensive flight envelope presents more challenges. Test data acquisition is expensive so maneuvers are designed for maximum efficiency and data quality with sometimes costly consequences. Verification methods are desired which accurately and efficiently include identification of critical parameters, address mismodeling and unmodeled dynamics, deal with test condition and system variability, and derive data-consistent parametric and nonparametric uncertainty descriptions (ref. [2, 3]). Non-parametric descriptions are addressed in this paper.

This paper attempts to approach estimation of ASE models with procedures to account for uncertainty, noise, and nonlinearity. Set membership identification in the form of bounded error estimation (ref. [2, 4]) has been used previously to characterize feasible sets of parameters with uncertainty estimates consistent

with the data, model structure, and prior information on uncertainty bounds. Minimum upper error bounds computed with parameter estimates result in a feasible set described as a function of the error bounds, thereby resulting in error bounds describing a smallest non-empty feasible set. These error bounds can be refined with appropriate data decompositions which extract relevant features from a time-frequency perspective.

Extraction of local time and frequency content of signals has been shown to be useful in nonstationary signal analysis for classification, recognition, and interpretation (ref. [5, 6]). Automated techniques are being pursued to detect impulsive, wide-band, and harmonic components by adaptive tracking of time-frequency and time-scale variations of multi-component signals (ref. [7, 8, 9]). Best basis algorithms seek to generate fast adaptive sparse representations that have enhanced resolution compared to non-adaptive approaches. These atomic decompositions act on overcomplete dictionaries for more general analysis over a wide class of signals (ref. [10, 11]). However, adaptive time-frequency localization is more efficient with orthogonal or approximately orthogonal data decompositions that project signals onto functions that form an orthonormal basis of finite energy signals (ref. [12, 7, 13]).

Application of an adaptive orthogonal data decomposition is used here to optimally extract information content. One technique uses a fast adaptive best-basis expansion of signals in local trigonometric bases (ref. [12, 14])(LTBs). Another near-orthogonal redundant wavelet basis (ref. [7, 15, 16, 17]) is also used for nonstationary time-frequency representations. Transfer functions are derived to demonstrate a less conservative uncertainty bound for robust stability analysis when using these signal representations.

These signal representations are incorporated in a nonlinear multiwavelet-based Volterra kernel identification procedure (ref. [18, 19]) to discern nonlinear-plus-noise dynamics from a best underlying linear representation. Kernels are identified from wavelet-processed data and discussion is presented about the applicability and feasibility of identifying Volterra kernels from nonlinear F/A-18 Active Aeroelastic Wing (ref. [20]) flight data.

AEROSERVOELASTIC DATA ANALYSIS

The ASE open-loop plant model includes rigid body and elastic modes, coupled high-order actuator dynamics, and control surface modal dynamics (ref. [3]). Including the aerodynamic lag states, the ASE state equations are

$$\dot{x} = Ax + Bu, \quad y = Cx + Du; \quad x = \lceil \eta_\delta \eta_r \eta_e \dot{\eta}_r \dot{\eta}_e \eta_a \delta \rfloor$$

consisting of input control surface commands u, actuator states η_δ, rigid body states η_r, flexible mode states η_e, aerodynamic lag states η_a, and control surface displacements δ. Aeroservoelastic plant, P, is therefore represented as the state-space operator. Associated with this time-domain representation is the transfer function, $P(s)$, a function of the complex Laplace variable, s, such that $y = P(s)u$, where $P(s) = D + C(sI - A)^{-1}B$. Controller $K(s)$ is modeled similarly, but being a digital implementation, it is modeled as a function of discrete complex variable, z, as $K(z = e^{sT})$ specified by the sampling time T and a zero-order sample-hold at the input of the controller.

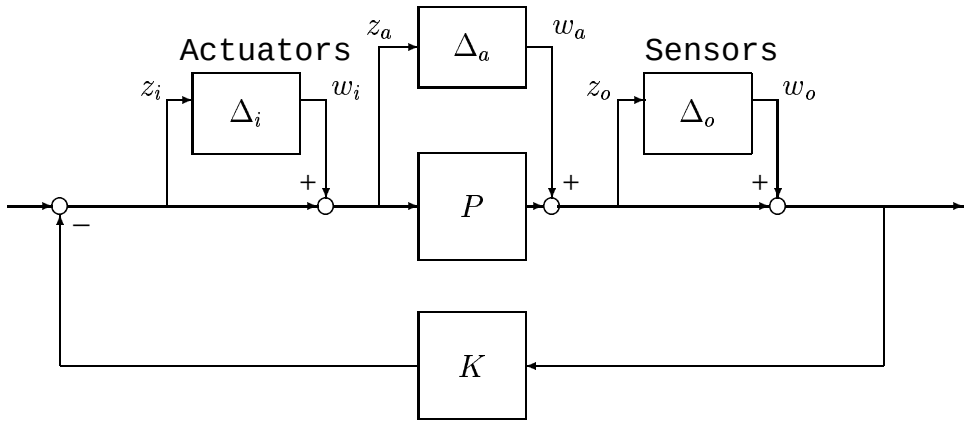

Figure 1: Closed-loop ASE model with additive and multiplicative plant uncertainty.

Multiplicative uncertainty is used to represent unmodeled dynamics and errors from the feedback sensors ($w_o = \Delta_o z_o$) and actuator input commands ($w_i = \Delta_i z_i$) as shown in Figure 1. Each of Δ_o and Δ_i are diagonal complex perturbations of appropriate output or input dimensions, with suitable weights W_i such that the uncertainty pertubations are norm-bounded by unity. Multiplicative perturbation at the output results in perturbed model $\tilde{P}_o = (I + \Delta_o)P$, and at the input the perturbed model is $\tilde{P}_i = P(I + \Delta_i)$. Structured robust stability tests representing these types of uncertainty are described from the complementary sensitivity matrix functions of complex $P(s)$ and $K(s)$, namely, $T_o = PK(I + PK)^{-1}$ and $T_i = KP(I + KP)^{-1}$. Another uncertainty characterization is the additive perturbation, Δ_a, with perturbed plant $\tilde{P}_a = P + \Delta_a$, which is depicted in Figure 1 ($w_a = \Delta_a z_a$). The effect of real parametric uncertainty at the plant input or output can be shown to represent an additive uncertainty in the plant transfer function (ref. [2]). Necessary and sufficient conditions for structured robust stability are then derived from the following tests on loop sensitivity functions (ref. [21, 22]) (where $\|\Delta_o\|_\infty < 1$, $\|\Delta_i\|_\infty < 1$, and $\|\Delta_a\|_\infty < 1$) with the structured singular value, μ, depending on the type of uncertainty, $\{\Delta_i, \Delta_o, \Delta_a\}$.

$$\mu_{\Delta_o}(W_2 T_o W_1) \leq 1, \quad \mu_{\Delta_i}(W_4 T_i W_3) \leq 1, \quad \mu_{\Delta_a}(W_6 K(I + PK)^{-1} W_5) \leq 1.$$

Data Decompositions

An uncertainty bound estimation technique based on robust minimax estimation (ref. [2, 4]) is used here to demonstrate the effects of signal representations on robust stability analysis. Minimum upper error bounds are computed with the ASE model parameter estimates such that the feasible estimation set is described as a function of the error bounds with no apriori assumption on the noise or model uncertainty. Transfer functions are computed in the robust minimax estimation scheme to identify input-output parameters and structured error bounds consistent with the data. These uncertainty estimates provide structured uncertainty representations for robust stability analysis useful for model validation and control system design.

Two types of data decompositions (projections of the data onto a set of pre-defined basis functions) to be discussed in this paper are of concern for either linear or nonlinear signal analysis and system identification. Many other options (ref. [10, 8, 9, 11, 23]) based on time-frequency filtering, localization, and wavelet denoising (ref. [13]) ideas have shown promise for signal enhancement, interpretation, and analysis, and will be pursued for ASE flight test dynamics in future research. The two chosen in this paper, (1) local trigonometric (ref. [12]) and, (2) Morlet wavelet (ref. [15, 16]) bases, are illustrative of other methods and have sound theoretical and practical justification.

Local time-frequency signal decompositions generally require basis functions well localized in both time and frequency. Orthogonality helps for algorithmic efficiency. An adaptive decomposition is desired for better accuracy and sparsity in the representation. Signals are projected onto orthonormal bases each with different time-frequency properties before choosing the best basis with some (information cost) optimality criteria. Popular and fast algorithms for best-basis selection include wavelet packets (ref. [14]) which allow for a general basis representaion but usually require a dyadic decimation at each scale, and it can be difficult to relate coefficients between scales or from a scale to the original signal. LTBs have excellent time and frequency resolution and allow for simple and fast algorithms (ref. [12, 13, 14]) while relying only on trigonometric functions, which may not be appropriate for signals of interest.

LTBs assign a ramp, or rising cutoff function $r(t) = \exp[\jmath\rho(t)]\sin[\theta(t)]$, which rises from zero to unity in the interval $\{-1, 1\}$ for $\rho \in \{2n\pi, 2m\pi\}$ and $\theta \in \{0, \frac{\pi}{2}\}$. Windows are created from the ramp functions applied to both sides of each interval. Local cosines are constructed by dilating, normalizing, and translating windowed block cosines over a disjoint partition of intervals of the signal. Cosines and/or sines are then used as bases to orthogonally project the data onto compactly supported windowed trigonometric functions which are well-localized in time and frequency. Adaptivity depends on best-basis algorithms choosing optimal partitions and corresponding coefficients for the expansion. A reasonable criteria is the decay rate of coefficients as a function of the partition, which is quantified by the derivatives locally at the intervals. Based on this criteria the decision to divide intervals is made locally independent of other changes (ref. [12]). By using the Fourier transform property of derivation, $< f^m, e^{-\jmath\pi n/|I|} >= (-\jmath\pi n/|I|)^m < f, e^{-\jmath\pi n/|I|} >$ for partition length $|I|$, the algorithm is efficient.

Wavelet decompositions also have desirable properties for signal decompositons if the wavelet basis functions have properties inherent to the signal. Morlet wavelet multiresolution analysis can provide efficient (well-matched to the signal) and descriptive coefficients for feature detection and identification purposes (ref. [7, 24, 16]) much like the LTBs for sinusoidal-like signals.

Results

Flutter and ASE clearance in both the subsonic and supersonic envelopes for the Active Aeroelastic Wing is accomplished with multisine sweeps summed to pertinent actuator commands, as was done previously on the NASA Dryden F/A-18 Systems Research Aircraft (ref. [2]). The 56 structural accelerometers are distributed on the fuselage, empennages, and all control surfaces. Control system feedbacks, commands, and surface positions are also available for ASE monitoring. Demonstration of the effect of signal decompositions into the LTBs and the Morlet wavelet functions will now be demonstrated.

This paper is concerned with ASE stability estimation and aeroelastic dynamics identification with signals represented as in Figure 2. Here is the right rear-wingtip accelerometer response at Mach0.85, 15,000ft altitude during a multisine input to the collective aileron command. The sweeps run from 3-35Hz for 26sec, and this segment is a portion between 5-10sec during excitation of the first symmetric wing bending mode. The top plot is the raw data at 200sps and the second plot is LTB-filtered with a hard denoising threshold of the LTB coefficients at 90% (ref. [12]). Hard thresholding corresponds to an optimization of the signal into a best basis by minimizing the residual norm amongst all data sets with a fixed number of nonzero coefficients determined by the threshold (ref. [11]). Despite this extreme threshold, the signal looks remarkably similar to the original. However, the LTB-filtered signal must correspond to a trigonometric basis, and the residual shown on the same plot (second from the top) is white noise.

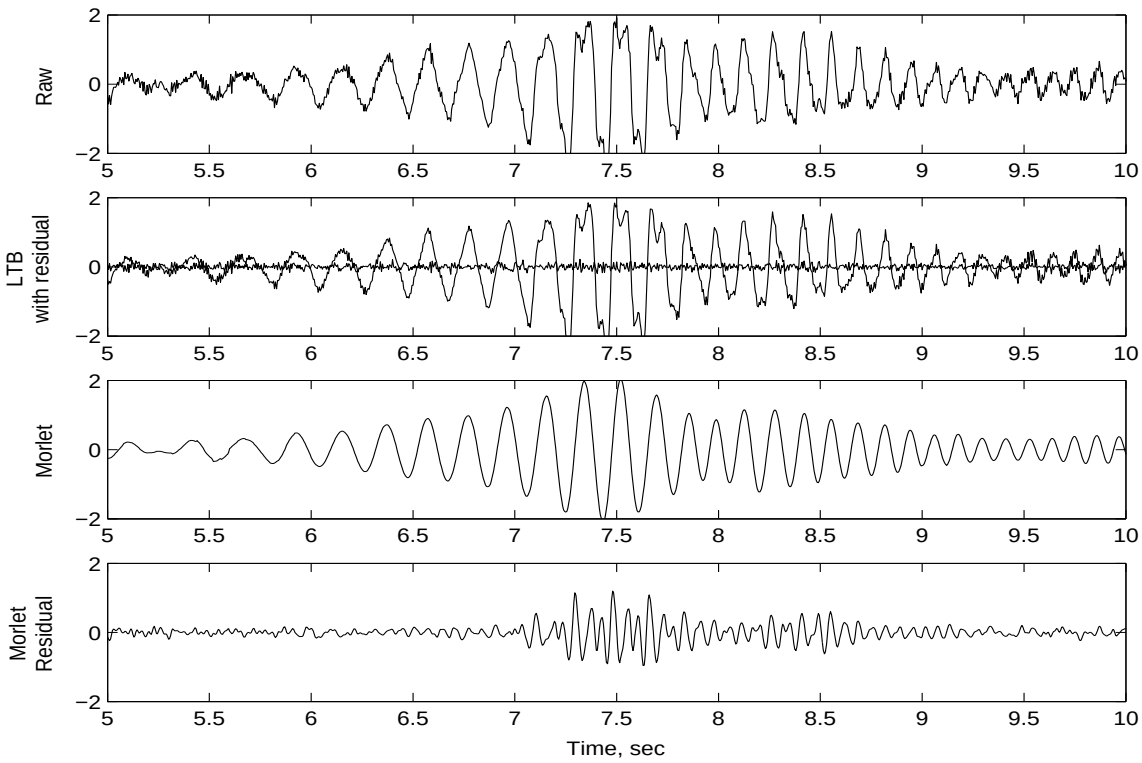

Figure 2: AAW right rear-wingtip accelerometer response (g's) of first symmetric wing bending mode from multi-sine excitation to the symmetric aileron command. From top to bottom:
Raw data, LTB-filtered with residual, Morlet-filtered, and residual of Morlet-filtered signal.

The Morlet-filtered data in the third plot of Figure 2 is clearly a sinusoidal basis of the data in-phase with the original signal. A residual of the Morlet wavelet coefficients in the fourth plot is calculated as the signal reconstruction from the coefficients that are not used in the reconstruction of the filtered signal of the third plot. These residual wavelet coefficients are extracted from the scalogram (time-frequency map of the wavelet coefficients) outside the region of the input signal. Hence, these contributions are due to extraneous signal content outside of the commanded input multisine sweep such as from exogenous input, nonlinearity, and noise in the response. These Morlet-derived signal representations will assist in linear vs nonlinear dynamics identification using Volterra kernels in the next section.

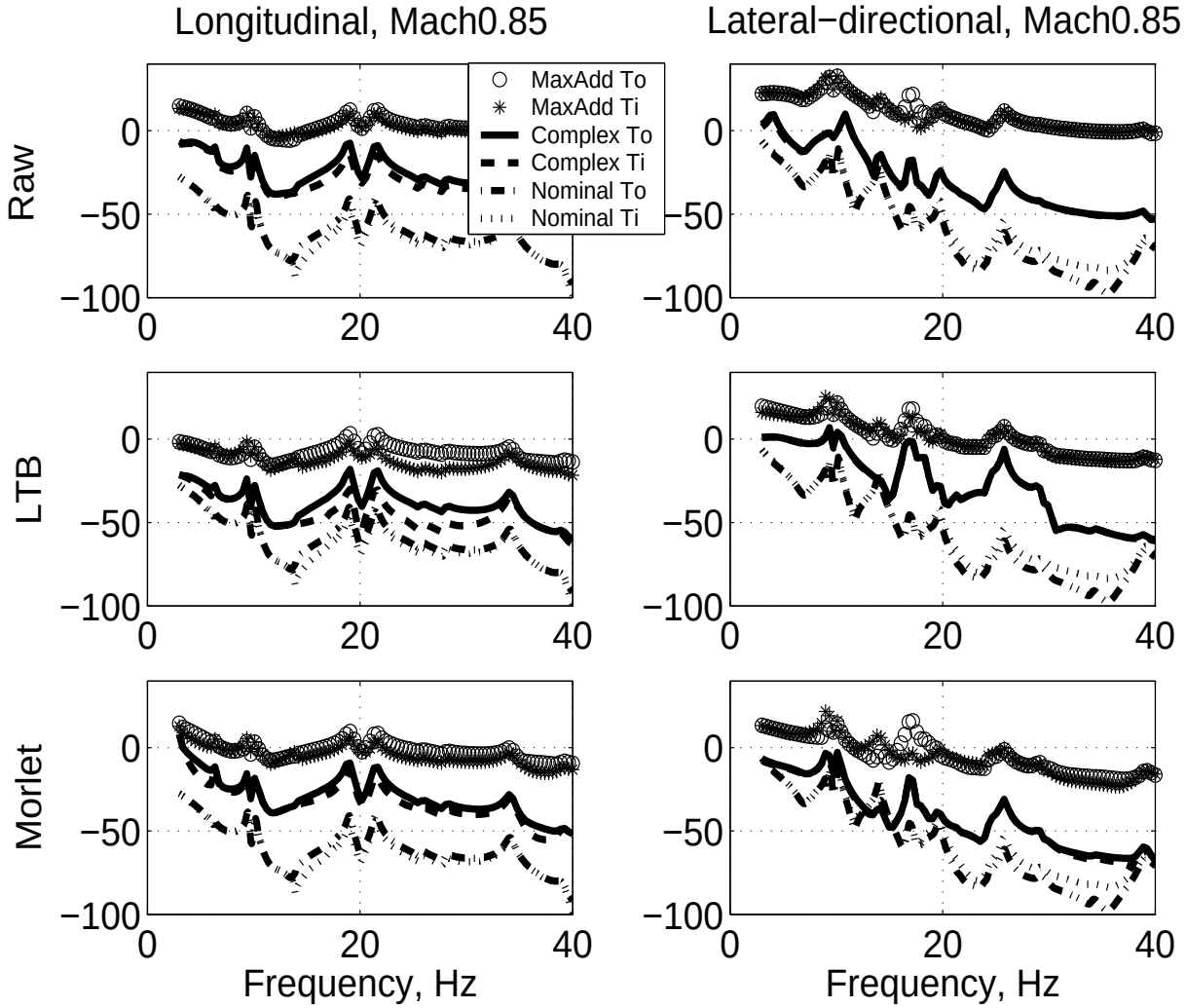

Figure 3: Mach0.85, 5,000 feet; Additive perturbation analysis (MaxAdd), complex multiplicative (Complex), and nominal (Nominal) model analysis using complentary sensitivity functions T_i and T_o.
Left plots are longitudinal analyses, and right plots are lateral-directional analyses.
Raw data (top), LTB-filtered data (middle), and Morlet-filtered data (bottom).

To demonstrate the effects of these signal representations on stability analysis, the raw data, LTB-filtered data, and Morlet-filtered feedback responses and control commands are used to compute the complementary sensitivity functions $\{T_i, T_o\}$ and perform the structured robust stability analyses represented by Figure 1 and expressions (1). In the top plots of Figure 3 and Figure 4, raw data from two flight conditions are chosen for longitudinal and lateral-directional robust stability analyses. These conditions are chosen as a transonic (Mach0.95, 15K feet) and a highly turbulent (Mach0.85, 5K feet) case. Multisine inputs are aileron, outboard leading edge, collective stabilator, and rudder commands, and outputs are normal and lateral acceleration, roll rate, pitch rate, and yaw rate feedbacks. Additive perturbation analysis (MaxAdd) uses Δ_a from Figure 1 derived from the data, complex multiplicative (Complex) analysis is derived from updated transfer functions and $\{\Delta_i, \Delta_o\}$ from (1) based on corrections to the nominal models to match the data in a minmiax optimization procedure (ref. [2, 4]), and the nominal (Nominal) analysis is

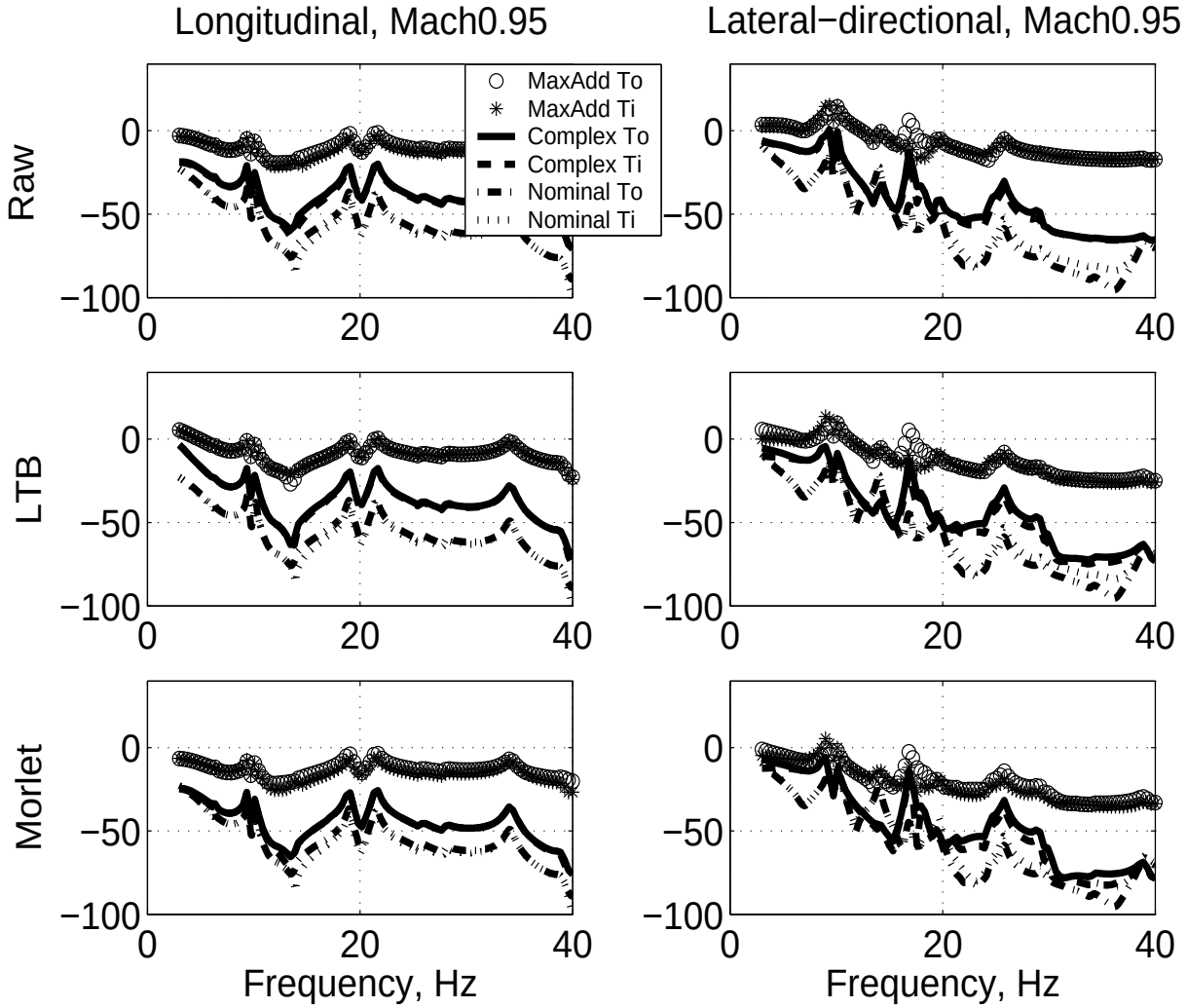

Figure 4: Mach0.95, 15,000 feet; Additive perturbation analysis (MaxAdd), complex multiplicative (Complex), and nominal (Nominal) model analysis using complentary sensitivity functions T_i and T_o.
Left plots are longitudinal analyses, and right plots are lateral-directional analyses.
Raw data (top), LTB-filtered data (middle), and Morlet-filtered data (bottom).

also complex multiplicative uncertainty analysis at the input and output from the baseline analysis models.

Note the large errors between nominal and updated models at Mach0.85, and high gain levels in the lateral-directional responses near 10Hz (near and above 0dB, and large uncertainty). Since the time-domain data does not indicate a tendency towards resonance or instability, the responses are suspect due to turbulence levels or transonic effects. LTB-filtered data is used to generate the responses in the middle plots of Figures 3 and 4, where there is much improvement in the longitudinal uncertainty levels and matches between updated and nominal models at Mach0.85, and some improvement in the still-conservative gain levels of the lateral-directional responses.

Finally, in the bottom plots of Figure 3 and Figure 4 it is shown that the Morlet-filtered results gener-

ally produce less conservative stability margin and more realistic lateral-directional gain levels where the modal peaks near 10Hz are more reasonable with reference to the flight data. This shows a reasonable improvement in the Morlet-filtered responses especially in the transonic and lateral-directional comparisons with raw and LTB-filtered data.

NONLINEAR AEROELASTIC DATA ANALYSIS

Volterra series representations provide a convenient framework for the analysis of nonlinear dynamical systems. The Volterra theory of nonlinear systems states that the system output y can be expressed in terms of an infinite series of integral operators of increasing order (ref. [25]). In practice, the series is truncated and this paper considers Volterra models that include only the first and second-order operators. For a causal, time-invariant, single-input/single-output system, the first and second-order Volterra operators take the form

$$y_1(t) = \int_0^t h_1(\xi)u(t-\xi)d\xi \tag{1}$$

$$y_2(t) = \int_0^t \int_0^t h_2(\xi,\eta)u(t-\xi)u(t-\eta)d\xi d\eta \tag{2}$$

where u is the input and h_1, h_2 are the first and second-order Volterra kernels. Collectively, the Volterra kernels provide a model of the system since, once the kernels have been identified, the response to any arbitrary input can be determined. The first-order kernel represents the linear dynamics of the system while the kernels of second-order and higher characterize the nonlinear dynamics. It should be noted that, for a linear system, the first-order kernel is equivalent to the impulse response of the system and the output is given by equation (1). Therefore, the Volterra theory can be viewed as an extension of the concept of linear convolution to nonlinear systems. In general, Volterra series are applicable to systems that exhibit fading memory. Fading memory asserts that past inputs have a diminishing influence on the present output. This implies that all of the Volterra kernels of a given system decay to zero in a finite period of time.

Volterra kernel identification

The difficulty in using Volterra series to model dynamical systems lies in the identification of the Volterra kernels. Fundamentally, kernel identification is an ill-posed, inverse problem since the objective is to determine the system model from input and output measurements. Also, a large number of coefficients are often needed to represent Volterra kernels, with the number increasing geometrically with the order of the kernel. For example, a discrete Volterra model requires on the order of N^p coefficients to represent the pth-order kernel for an N-dimensional data set. In view of these limitations, many different approaches have been taken to identify Volterra kernels in both the time and frequency domains. Direct measurement techniques have been employed whereby the kernels are identified in terms of the response of the system to specific inputs. These include harmonic probing and the application of impulsive inputs to discrete-time

systems (ref. [26]). Many approaches are statistical in nature and can be viewed as variations of the cross-correlation technique developed by Lee and Schetzen (ref. [27]) for Gaussian white noise inputs. Other methods, including the approach taken in this paper, seek to expand the kernels in terms of a relatively small number of basis functions such as Laguerre polynomials (ref. [28]) or decaying exponentials (ref. [29]).

In this paper, orthonormal, piecewise-polynomial multiwavelets are used to approximate the first and second-order kernels of nonlinear aeroelastic systems. Wavelets are compactly-supported, oscillatory functions that are constructed to satisfy certain properties such as orthogonality, smoothness, and symmetry requirements (ref. [13]). Multiwavelets compose a set of wavelet functions $\{\psi^1, \ldots, \psi^r\}$ that are generated from a set of scaling functions $\{\phi^1, \ldots, \phi^r\}$ (ref. [30]). The scaled translates and dilates of the multiwavelets form a basis for $L^2(\mathbb{R})$, the space of square-integrable functions. The scaling functions generate a multiresolution analysis, a series of nested approximation spaces $\{V_j\}_{j\in\mathbb{Z}}$. Each space V_j is defined as

$$V_j := span\left\{\phi^s_{j,k} : \ k \in \mathbb{Z}, \ s \in \{1, \ldots, r\}\right\}$$

where

$$\phi^s_{j,k} = 2^{j/2}\phi^s(2^j - k)$$

Hence, increasing the dilation index j by one effectively doubles the resolution of the space V_j. The translation index k gives the position of the function on the real line. The multiwavelets are constructed so that they span the orthogonal complement spaces $\{W_j\}$:

$$W_j = V_{j+1} \ominus V_j, \ \ j \in \mathbb{Z} \tag{3}$$

Each wavelet space W_j is defined as

$$W_j := span\left\{\psi^s_{j,k} : \ k \in \mathbb{Z}, \ s \in \{1, \ldots, r\}\right\}$$

where

$$\psi^s_{j,k} = 2^{j/2}\psi^s(2^j - k)$$

Applying equation (3) recursively, the approximation space V_{j+1} can be decomposed as

$$V_{j+1} = W_j \oplus W_{j-1} \oplus \cdots \oplus W_{j_0} \oplus V_{j_0} \tag{4}$$

where j_0 is the coarsest resolution level in the decomposition.

This paper employs piecewise-quadratic multiwavelets that have been constructed using the technique of intertwining (ref. [30]). This process derives four scaling functions and associated multiwavelets from the classical quadratic finite element basis functions. The details of this construction and plots of the multiwavelets are given in Ref. [18]. This class of multiwavelets is well-suited for the approximation of Volterra kernels because the functions are orthogonal, symmetric or antisymmetric, and are easily adapted to the finite domains over which the kernels are supported.

In using these multiwavelets for kernel identification, the first-order kernel is first written in terms of a fine-resolution approximation space V_j as

$$h_{1,j}(\xi) = \sum_{s=1}^{4}\sum_{k} \alpha^s_{j,k}\phi^s_{j,k}(\xi) \tag{5}$$

where $\{\alpha^s_{j,k}\}$ are constant coefficients. Equation (4) implies that an equivalent, multiscale representation of the kernel can be obtained as

$$h_{1,j}(\xi) = \sum_{l=j_0}^{j-1} \sum_{s=1}^{4} \sum_{k} \beta^s_{l,k} \psi^s_{l,k}(\xi) + \sum_{s=1}^{4} \sum_{k} \alpha^s_{j_0,k} \phi^s_{j_0,k}(\xi)$$

This multiscale representation, termed the discrete wavelet transform, is desirable because it decomposes the kernel into a coarse-scale average over V_{j_0} and a series of details of varying resolution over the wavelet spaces $W_{j_0}, \ldots, W_{j-1}$. Furthermore, many of the coefficients in the multiscale expansion are often close to zero and can be neglected, leading to a sparse representation. The kernel identification problem is easier to formulate in terms of the single-scale representation in equation (5). Fast, recursive algorithms are then applied to relate the single-scale coefficients to the multiscale wavelet coefficients.

In a similar manner, the second-order kernel is expanded in terms of two-dimensional scaling functions and multiwavelets. These two dimensional functions are obtained as the tensor products of the one-dimensional scaling functions and wavelets. A single-scale approximation of the second-order kernel can be written as

$$h_{2,j}(\xi,\eta) = \sum_{s,t=1}^{4} \sum_{k,m} \alpha^{s,t}_{j,(k,m)} \phi^s_{j,k}(\xi) \phi^t_{j,m}(\eta) \tag{6}$$

and the equivalent multiscale expansion is given by

$$\begin{aligned} h_{2,j}(\xi,\eta) &= \sum_{s,t=1}^{4} \sum_{k,m} \alpha^{s,t}_{j_0,(k,m)} \phi^s_{j_0,k}(\xi) \phi^t_{j_0,m}(\eta) + \sum_{l=j_0}^{j-1} \sum_{s,t=1}^{4} \sum_{k,m} \beta^{1,(s,t)}_{l,(k,m)} \phi^s_{l,k}(\xi) \psi^t_{l,m}(\eta) \\ &+ \sum_{l=j_0}^{j-1} \sum_{s,t=1}^{4} \sum_{k,m} \beta^{2,(s,t)}_{l,(k,m)} \psi^s_{l,k}(\xi) \phi^t_{l,m}(\eta) + \sum_{l=j_0}^{j-1} \sum_{s,t=1}^{4} \sum_{k,m} \beta^{3,(s,t)}_{l,(k,m)} \psi^s_{l,k}(\xi) \psi^t_{l,m}(\eta) \end{aligned} \tag{7}$$

It has been shown that the Volterra kernels can be assumed to be symmetric. Under this assumption, the number of unique coefficients in equations (6) and (7) can be reduced by almost a factor of two.

The multiwavelet representations of the first and second-order kernels are substituted into equations (1) and (2), respectively. Then, using a zero-order hold approximation of the input and output, the kernel identification problem reduces to the matrix equation

$$\underline{y}_j = \underline{y}_{1,j} + \underline{y}_{2,j} = [A_1 \ A_2] \left\{ \begin{array}{c} \underline{\beta}_1 \\ \underline{\beta}_2 \end{array} \right\} \tag{8}$$

(see Ref. [18] for details). In equation (8), $\underline{y}_j$ represents a vector of discrete outputs that have been sampled at 2^jsps and $\underline{y}_{1,j}, \underline{y}_{2,j}$ are vectors of discrete first and second-order outputs. The vectors $\underline{\beta}_1$ and $\underline{\beta}_2$ are composed of the multiscale wavelet coefficients that represent the first and second-order kernels. Equation (8) is solved, in a least-squares sense, for the first and second-order kernel coefficients. In many cases, the vectors $\underline{\beta}_1$ and $\underline{\beta}_2$ can be truncated to obtain reduced-order representations of the kernels.

Results

The multiwavelet-based Volterra kernel identification method was used to extract first and second-order kernels from AAW flight data. In previous work, a similar approach was applied to flight data from the Aerostructures Test Wing (ATW), a small-scale test wing that was designed to study flutter (ref. [19]). In that study, first-order kernels were successfully identified from the flight data at various flight conditions. The identified second-order kernels were essentially zero, indicating that the ATW was a predominantly linear system with two degrees-of-freedom. The AAW, on the other hand, is a much more complex system with many coupled degrees-of-freedom, and the flight data clearly indicates the presence of aeroelastic nonlinearities.

In practice, first and second-order Volterra kernels must be identified simultaneously because the terms in the Volterra series are not orthogonal. The Morlet wavelet filtering procedure can be used to simplify the identification procedure by decomposing the data into a linear component and a residual. The linear component is generated by correlating the input and output frequencies in the time domain. The portion of the output that matches the input frequencies is assumed to be linear. The residual data is assumed to be composed of nonlinear data and noise. In this manner, a good approximation of the linear and nonlinear portions of the response data is obtained. As an additional benefit, much of the noise in the data is removed during the Morlet filtering process. The first-order kernel is then identified from the Morlet-filtered data, and the second-order kernel is identified from the residual data. Of course, it is certainly possible that the Morlet-filtered data contains some nonlinear response at the input frequencies. Such response could be modeled in terms of odd-order kernels of third order and higher, which are not considered in this paper.

As an example, first and second-order kernels were extracted from AAW flight data at a flight condition of $15,000$ ft, Mach number 0.85. The input was a multisine collective aileron sweep and the output was taken as accelerometer data from the forward right wing just inside the wing fold. This data, which was sampled at 128 sps, is shown in Figure 5. It should be noted that the mean of both data sets has been removed to ignore variations in the trim condition during the maneuver. The Morlet filtering procedure was applied to the accelerometer data. The Morlet-filtered response and the residual are shown in Figure 6.

A first-order kernel was identified from the Morlet-filtered data, which was assumed to be linear. Then, a symmetric, second-order kernel was extracted from the residual data, which was assumed to be composed of nonlinear data and noise. The identified kernels are shown in Figure 7. The memory, or time duration, of each kernel was chosen by trial and error to be the minimum time for each kernel to decay to zero. Minimizing the kernel lengths reduces the number of coefficients that must be identified. This is especially significant for the second-order kernel, where doubling the memory would increase the number of coefficients by a factor of four. Similarly, the number of wavelet coefficients needed to represent each kernel, which is directly related to the number of levels of resolution used, was also determined via trial and error. Basically, the number of resolution levels was increased until the kernels converged and there was no benefit in including additional coefficients in the model. The first-order kernel shown in Figure 7 is composed of 257 wavelet functions and has a memory of 2 seconds. The symmetric second-order kernel is represented in terms of 561 unique wavelet coefficients and has a memory of 1 second.

The output predicted by the identified first-order kernel is shown in Figure 8. Also shown is a com-

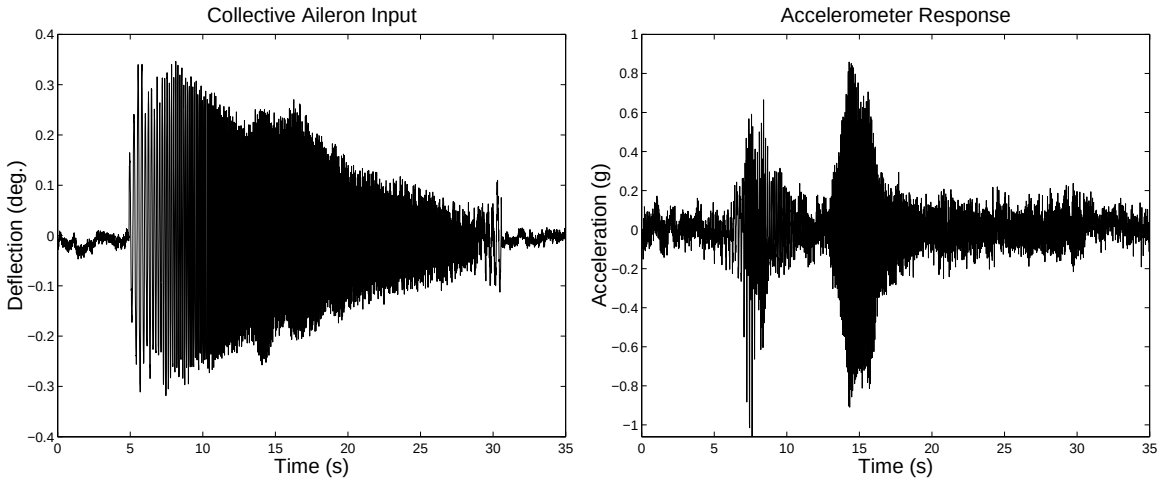

Figure 5: Collective aileron input and accelerometer response (right wing forward, inside wing fold) at flight condition Mach0.85, 15,000 ft.

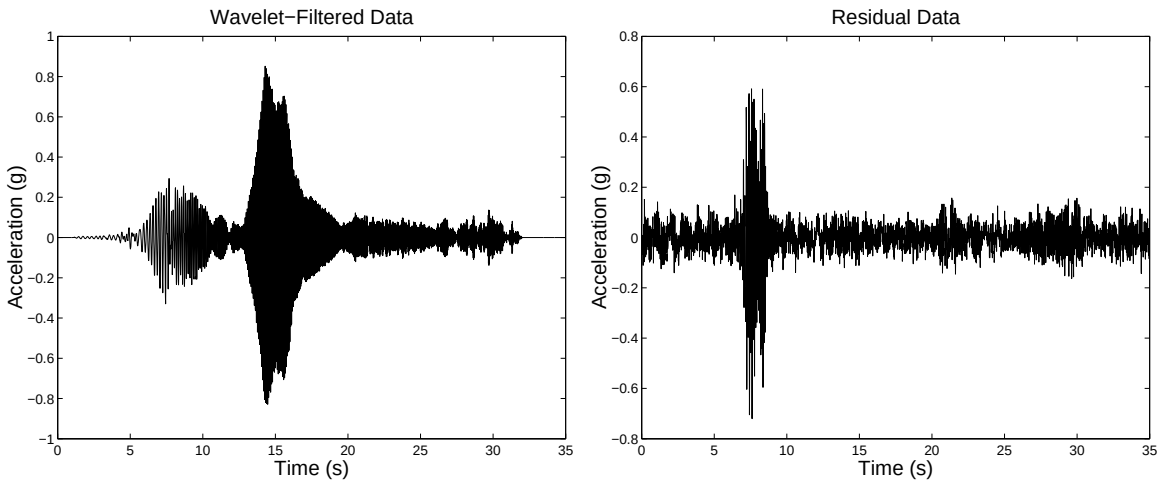

Figure 6: Morlet-filtered data and residual.

parison of the Morlet-filtered data and the identified first-order data over a small window in time, corresponding to the excitation of the 14 Hz mode. The identified output closely matches the Morlet-filtered data with some amplitude difference.

The response predicted by the identified second-order kernel is depicted in Figure 9. The predicted second-order response is mostly concentrated in the $6-9$ second time range. A detailed analysis of the residual data revealed significant 12 and 14 Hz responses corresponding to input frequencies of 6 and 7 Hz, respectively. This occurred in the time range of $6-9$ seconds and is clearly indicative of a quadratic nonlinearity. The fact that this response is evident in other data sets demonstrates that it is indeed due to a nonlinearity and not merely a linear response to external disturbances. As shown in the zoomed-in plot in Figure 9, the second-order kernel is able to predict this nonlinear response to a reasonable degree of accuracy.

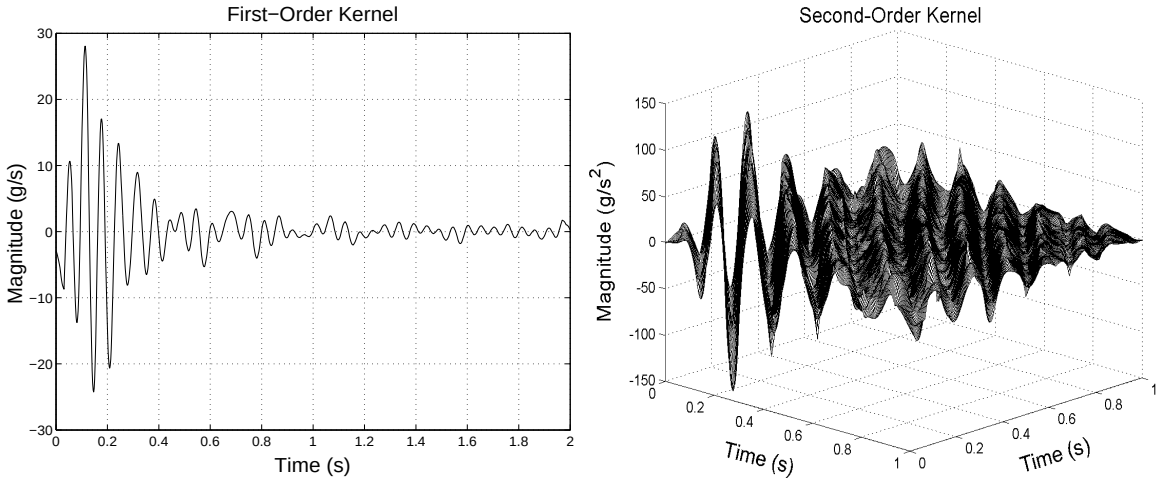

Figure 7: Identified first and second-order Volterra kernels.

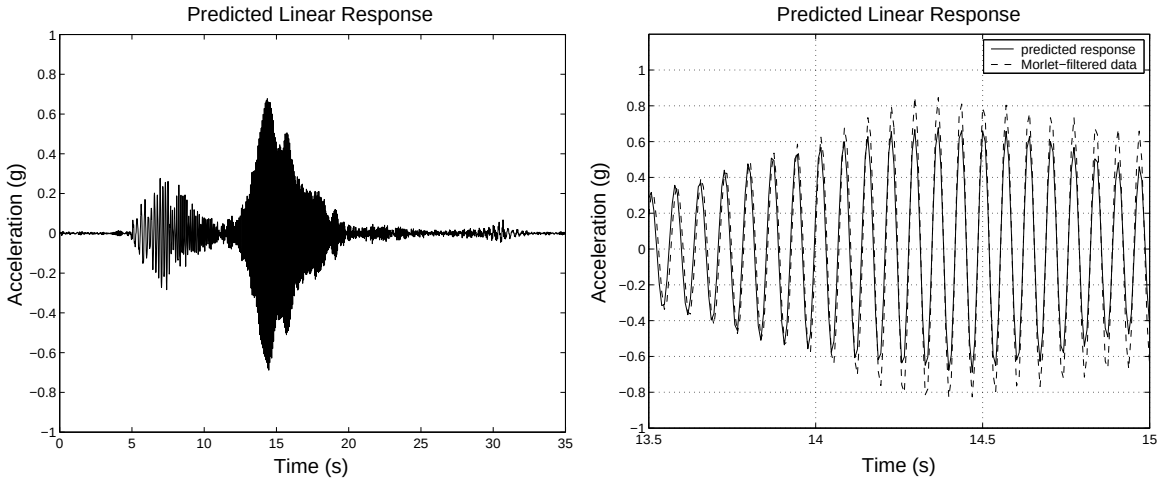

Figure 8: Linear output predicted by the identified first-order kernel.

CONCLUSIONS

Data decompositions are investigated for more reliable stability estimates while accounting for uncertainty, noise, and nonlinearity. Error bounds on the estimates are found to improve with nonstationary data processing methods which extract localized time and frequency content. Adaptive data decompositions offer a choice of basis functions for enhanced information extraction.

Morlet wavelet filtering provides a convenient decomposition of the data into a linear component and a residual composed of nonlinear response and noise. Volterra operators are designed with orthonormal, piecewise-polynomial multiwavelets to approximate the first and second-order kernels of nonlinear aeroelastic systems. This class of multiwavelets is well-suited for the approximation of Volterra kernels because the functions are orthogonal and are easily adapted to the finite domains over which the kernels are supported.

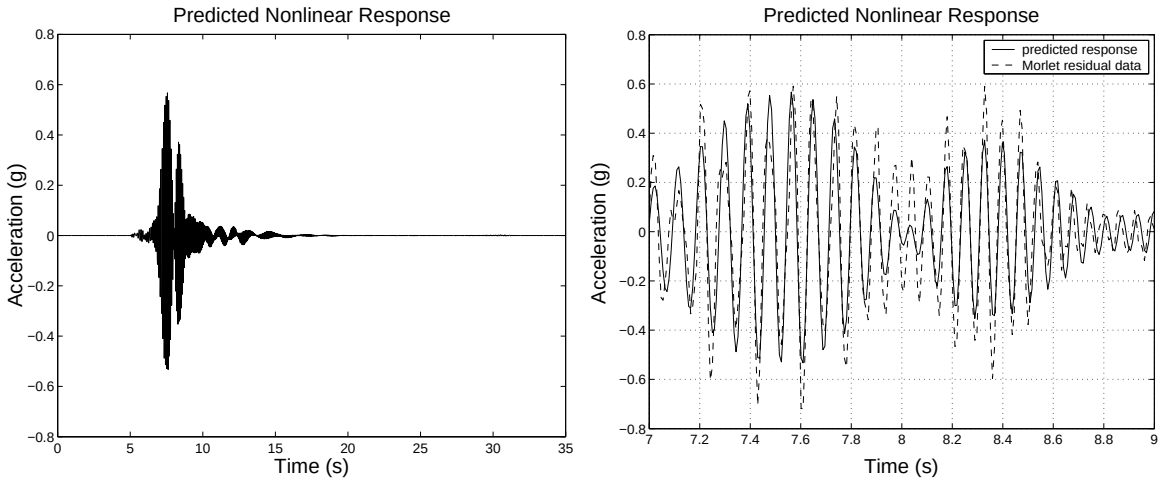

Figure 9: Nonlinear output predicted by the identified second-order kernel.

A first-order Volterra kernel is identified from filtered data to model the linear dynamics. The nonlinear dynamics are then modeled in terms of the second-order Volterra kernel, identified from the residual data. An example was given demonstrating the potential of this approach for obtaining reasonably accurate models of nonlinear aeroelastic systems with a relatively low number of wavelet basis functions.

Dryden Flight Research Center
National Aeronautics and Space Administration
Edwards, California, April 14, 2003

REFERENCES

1. Raveh, Daniella E., Y. Levy, and M. Karpel, "Efficient Aeroelastic Analysis Using Computational Unsteady Aerodynamics", *AIAA Journal of Aircraft*, **38**(3), May-Jun 2000, pp. 547-556.

2. Brenner, Martin J., "Aeroservoelastic Model Uncertainty Bound Estimation from Flight Data", *AIAA Journal of Guidance, Control, and Dynamics*, **25**(4), Jul-Aug 2002, pp. 748-754.

3. Lind, Rick and Marty Brenner, *Robust Aeroservoelastic Stability Analysis: Flight Test Applications*, Series: Advances in Industrial Control, Springer-Verlag, 1999.

4. Milanese, Mario, J. Horton, H. Piet-Lahanier, and É. Walter, Eds., *Bounding Approaches to System Identification*, Plennum Press, New York, 1996, pp. 183-197.

5. Leprette, Benoit, N. Martin, F. Glangeaud, and J.-P. Navarre, "Three-Component Signal Recognition Using Time, Time-Frequency, and Polarization Information – Application to Seismic Detection of Avalanches", *IEEE Transactions on Signal Processing*, **46**(1), Jan 1998, pp. 83-102.

6. Leprette, Benoit and N. Martin, "Extraction of pertinent subsets from time-frequency representations for detection and recognition purposes", *Signal Processing*, **82**(2002), pp. 229-238.

7. Brenner, Martin J., "Nonstationary Dynamics Data Analysis with Wavelet-SVD Filtering", *Mechanical Systems and Signal Processing*, accepted Jul 26, 2002.

8. Hory, Cyril, N. Martin, and A. Chehikian, "Spectrogram Segmentation by Means of Statistical Features for Non-Stationary Signal Interpretation", *IEEE Transactions on Signal Processing*, **50**(12), Dec 2002, pp. 2915-2925.

9. Klein, R., D. Ingman, and S. Braun, "Non-stationary Signals: Phase-energy Approach – Theory and Simulations", *Mechanical Systems and Signal Processing*, **15**(6), 2001, pp. 1061-1089.

10. Chen, Scott Shaobing, D.D. Donoho, and M.A. Saunders, "Atomic Decomposition by Basis Pursuit", SIAM Review, **43**(1), Mar 2001, pp. 129-159.

11. Sardy, Sylvain, P. Tseng, and A. Bruce, "Robust Wavelet Denoising", *IEEE Transactions on Signal Processing*, **49**(6), Jun 2001, pp. 1156-1152.

12. Borup, L. and M. Nielsen, "Fast adaptive expansions in local trigonometric bases", *Signal Processing*, **83**(2003), pp. 445-451.

13. Mallat, Stéphane, *A Wavelet Tour of Signal Processing*, Academic Press, 1999.

14. Wickerhauser, Mladen Victor, *Adapted Wavelet Analysis from Theory to Software*, A K Peters Ltd, Wellesley, MA, 1994.

15. Shensa, Mark J., "The Discrete Wavelet Transform: Wedding the À Trous and Mallat Algorithms", *IEEE Transactions on Signal Processing*, **40**(10), Oct 1992, pp. 2464-2482.

16. Shensa, Mark J., “Discrete Inverses for Nonorthogonal Wavelet Transforms”, *IEEE Transactions on Signal Processing*, **44**(4), Apr 1996, pp. 798-807.

17. Vetterli, Martin and Jelena Kovačević, *Wavelets and Subband Coding*, Prentice-Hall, Upper Saddle River, NJ, 1995, pp. 357-361.

18. Prazenica, Richard J., “Wavelet-Based Volterra Series Representations of Nonlinear Dynamical Systems”, Ph.D. Dissertation, University of Florida, Gainesville, FL, 2002.

19. Prazenica, Richard J., R. Lind and A. Kurdila, “ Uncertainty Estimation from Volterra Kernels for Robust Flutter Analysis”, *Proceedings of 43rd AIAA Structures, Structural Dynamics, and Materials Conference*, Denver, CO, AIAA-2002-1650.

20. Pendleton, E., D. Bessette, P. Field, G. Miller, and K. Griffin, “Active Aeroelastic Wing Flight Research Program: Technical Program and Model Analytical Development”, *AIAA Journal of Aircraft*, **37**(4), Jul-Aug 2000, pp. 554-561.

21. Balas, Gary J., et. al., *μ-Analysis and Synthesis Toolbox*, MUSYN, Inc. and The Mathworks, Inc., 1998.

22. Zhou, Kemin with John C. Doyle, *Essentials of Robust Control*, Prentice-Hall, Upper Saddle River, NJ, 1998.

23. Young, Ian T., L.J. van Vliet, and M. van Ginkel, “Recursive Gabor Filtering”, *IEEE Transactions on Signal Processing*, **50**(11), Nov 2002, pp. 2798-2805.

24. Ho, K.C. and Y.T. Chan, “Filter Design and Comparison for Two Fast CWT Algorithms”, *IEEE Transactions on Signal Processing*, **47**(11), Nov 1999, pp. 3013-3026.

25. Schetzen, M., *The Volterra and Wiener Theories of Nonlinear Systems*, John Wiley & Sons, 1980.

26. Silva, W., “Application of Nonlinear Systems Theory to Transonic Unsteady Aerodynamic Responses”, *Journal of Aircraft*, **30**(5), Sept-Oct 1993, pp. 660-668.

27. Lee, Y.W. and M. Schetzen, “Measuring of the Wiener Kernels of a Non-Linear System by Cross-Correlation”, *International Journal of Control*, **2**(3), 1965, pp. 237-254.

28. Marmarelis, V.Z., “Identification of Nonlinear Biological Systems Using Laguerre Expansions of Kernels”, *Annals of Biomedical Engineering*, **21**, 1993, pp. 573-589.

29. Reisenthel, P., “Prediction of Unsteady Aerodynamic Forces Via Nonlinear Kernel Identification”, *CEAS/AIAA/ICASE/NASA Langley IFASD*, June 1999.

30. Donovan, G., J. Geronimo, and D. Hardin, “Intertwining Multiresolution Analyses and the Construction of Piecewise-Polynomial Wavelets”, *SIAM Journal of Mathematical Analysis*, **27**(6), Nov 1996, pp. 1791-1815.

REPORT DOCUMENTATION PAGE

Form Approved
OMB No. 0704-0188

Public reporting burden for this collection of information is estimated to average 1 hour per response, including the time for reviewing instructions, searching existing data sources, gathering and maintaining the data needed, and completing and reviewing the collection of information. Send comments regarding this burden estimate or any other aspect of this collection of information, including suggestions for reducing this burden, to Washington Headquarters Services, Directorate for Information Operations and Reports, 1215 Jefferson Davis Highway, Suite 1204, Arlington, VA 22202-4302, and to the Office of Management and Budget, Paperwork Reduction Project (0704-0188), Washington, DC 20503.

1. AGENCY USE ONLY (Leave blank)

2. REPORT DATE
April 2003

3. REPORT TYPE AND DATES COVERED
Technical Memorandum

4. TITLE AND SUBTITLE
Aeroservoelastic Model Validation and Test Data Analysis of the F/A-18 Active Aeroelastic Wing

5. FUNDING NUMBERS
WU 710 61 14 SE 14 00 AAW

6. AUTHOR(S)
Martin J. Brenner and Richard J. Prazenica

7. PERFORMING ORGANIZATION NAME(S) AND ADDRESS(ES)
NASA Dryden Flight Research Center
P.O. Box 273
Edwards, California 93523-0273

8. PERFORMING ORGANIZATION REPORT NUMBER
H-2526

9. SPONSORING/MONITORING AGENCY NAME(S) AND ADDRESS(ES)
National Aeronautics and Space Administration
Washington, DC 20546-0001

10. SPONSORING/MONITORING AGENCY REPORT NUMBER
NASA/TM-2003-212021

11. SUPPLEMENTARY NOTES
Also to be presented at the CEAS/AIAA/NVvL International Forum on Aeroelasticity and Structural Dynamics 6/4/03 to 6/6/03, Amsterdam, The Netherlands. Author edited.

12a. DISTRIBUTION/AVAILABILITY STATEMENT
Unclassified—Unlimited
Subject Category 08

This report is available at http://www.dfrc.nasa.gov/DTRS/

12b. DISTRIBUTION CODE

13. ABSTRACT (Maximum 200 words)

Model validation and flight test data analysis require careful consideration of the effects of uncertainty, noise, and nonlinearity. Uncertainty prevails in the data analysis techniques and results in a composite model uncertainty from unmodeled dynamics, assumptions and mechanics of the estimation procedures, noise, and nonlinearity. A fundamental requirement for reliable and robust model development is an attempt to account for each of these sources of error, in particular, for model validation, robust stability prediction, and flight control system development. This paper is concerned with data processing procedures for uncertainty reduction in model validation for stability estimation and nonlinear identification. F/A-18 Active Aeroelastic Wing (AAW) aircraft data is used to demonstrate signal representation effects on uncertain model development, stability estimation, and nonlinear identification. Data is decomposed using adaptive orthonormal best-basis and wavelet-basis signal decompositions for signal denoising into linear and nonlinear identification algorithms. Nonlinear identification from a wavelet-based Volterra kernel procedure is used to extract nonlinear dynamics from aeroelastic responses, and to assist model development and uncertainty reduction for model validation and stability prediction by removing a class of nonlinearity from the uncertainty.

14. SUBJECT TERMS
Aeroservoelasticity, Local trigonometric basis, Morlet wavelet, Multiwavelet-based Volterra kernel identification, Robust minimax estimation,

15. NUMBER OF PAGES
21

16. PRICE CODE
A03

17. SECURITY CLASSIFICATION OF REPORT	18. SECURITY CLASSIFICATION OF THIS PAGE	19. SECURITY CLASSIFICATION OF ABSTRACT	20. LIMITATION OF ABSTRACT
Unclassified	Unclassified	Unclassified	Unlimited